AL21 - Impact of Slot Inclination and Thickness on the Distribution of Gas Bubbles Generated below the Anode

Mostafa El Mehdi Brik[1], Ievgen Necheporenko[2] and Alexander Arkhipov[3]
1. Engineer-I R&D
2. Engineer-I R&D
3. Manager – Modelling
Technology Development & Transfer department, Emirates Global Aluminium, Dubai, UAE
Corresponding author: mbrik@ega.ae

Abstract

This paper reports on a numerical study of the impact of the anode slot design on the evacuation and distribution of the electrolysis gases (mainly CO_2) generated at the bottom surface of the carbon anode in an aluminium electrolysis cell. Different slot inclinations (20 mm and 80 mm) and thicknesses (6 mm, 8 mm, 11 mm, and 22 mm) were investigated in this study, using COMSOL Multiphysics software based on the finite element method. The computational fluid dynamics (CFD) model consists of coupling turbulent flow and phase transport physics. The latter solves the phase transport equation and gives the gas volume fraction distribution in the computational domain, while the former gives principally the velocity and pressure profiles by solving the Navier-Stokes equation. The standard k-ε turbulence model is used. This study helps to understand the impact of the slot design on bath mixing in the central channel, affecting alumina dissolution, and side channels, affecting heat transfer to the walls and ledge profile. The outcomes are used to optimise slot designs in industrial cells.

Keywords: Aluminium electrolysis cell, Slotted carbon anode block, CFD, Bubble-induced turbulence.

1. Introduction

In industry, the production of primary aluminium consists of its reduction from alumina. This process occurs principally in an aluminium reduction cell called Hall- Héroult cell. Using direct electric (DC) current, aluminium oxide (alumina) is reduced in the molten electrolyte under high temperature (about 960 °C). This electrochemical reaction produces ideally aluminium (liquid metal) and oxygen O_2 (gas). The latter reacts with carbon anode and produces carbon dioxide gas (CO_2) bubbles at the bottom surface of the anode. The generation of such a gas phase induces bath circulation which helps, on one hand, dissolving alumina, and on the other hand, it increases heat transfer between the bath and the cell walls [1-3]. However, the existence of the gas bubbles for longer time underneath the anode block leads to their coalescence and forms a more continuous insulating gas layer, which increases electrical resistance in the anode-cathode distance (ACD) manifested as bubble voltage drop. The gas coverage of anode bottom surface increases with decreasing alumina concentration, reaching 80 % coverage when approaching the anode effect. Anode effect occurs at 1-2 % of alumina concentration in the bath; at this concentration another reaction occurs on the anode surface, generating perfluorocarbons (PFCs), which cover the entire anode bottom with a thin insulation layer, which increases cell resistance and cell voltage to typically 15-30 V [4]. To avoid formation of large bubbles many modifications of the anode shape, such as anode slots, have been performed in order to decrease the residence time of bubbles on the bottom surface of the anode block [5].

1.1 Experimental Studies

Several experimental works dealing with this subject are found in the literature. Because of the harsh operational conditions (high temperature, high electromagnetic field, and highly corrosive media), researchers have worked experimentally with other liquid-gas systems instead of cryolite-CO_2 system [6-8]. This approach is valid since the dynamic viscosity of other liquids at 25 °C is almost the same as that of the cryolite at 960 °C. Feng et al. [6], studied hydrodynamics of water under three anodes in presence of air injection to create bubble-induced turbulence). They used the particle image velocimetry (PIV) technique to measure the flow field. The results showed that, on one hand, the presence of slots in the anodes improved the hydrodynamics of the bath. On the other hand, the slots helped to quickly remove the gas from the bottom surface of the anode to the slots by which the gas easily evacuated to side channels. This contributes to increase mixing rates at the central and side channels. Other researchers [9-10] studied the dynamics of bubbles released from the bottom surface of graphite anodes in a molten bath of copper sulfate ($CuSO_4$). The results showed that the presence of a slot in the anode significantly increased the rate of bubble removal. The researchers attributed this to the fact that the slot created a pathway for the bubbles to rise to the surface more quickly.

1.2 Computational Fluid Dynamics (CFD)

With the remarkable development of the computational resources, researchers have focused on the CFD model development to better understand the mechanisms of gas bubble removal from the bottom surface of the anodes. Numerical models based on separated phases have been widely used in the treatment of this subject. Euler-Euler approach has been used by Hreiz et al. [11] to investigate the electro-generation of bubbles from a vertical electrode considering the impact of external forces as well as their coalescence. The generation of bubbles by the electric current applied to the cell was not present in their model because, as cited in the literature [11], it is difficult to ensure the convergence of the magnetohydrodynamic model based on Euler-Euler approach, contrary to Euler-Lagrange approach. The latter has been used by Hreiz et al. [12], where the electro-generation of bubbles function of the current density was considered in the model, that gave good agreement with experimental results obtained in parallel (using PIV). Wang et al. [13] proposed a CFD model based on volume of fluid (VOF) method to investigate the morphology of bubbles generated and released from the bottom surface of the anodes. In their model, researchers [13] neither included the force on the bubbles during their movement nor their coalescence in the bath. They showed that the slots provide the possibility for more gas removal. Sun et al. [14], proposed a 3D transient model that couples magnetohydrodynamics and VOF model to profoundly understand the effect of slotted anodes on bubble behaviour. The results showed that the time-averaged gas bubble removal rate increased from 36 to 63 % when using slotted anodes and the bubble layer thickness is reduced by about 3.5 mm (17.4 %). To go deeply in their study, Sun et al. [14] investigated the transition of bubble sizes and its coalescence from micro-to-macro-scale, coupling the discrete bubble model (DBM) and VOF method. The model results had good agreement with the experimental data existing in the literature [15]. They found principally that bubble release frequency increases with increasing current density. From the different studies cited above and others existing in the literature, researchers concluded that the study of the bath hydrodynamics is likely to be complex and related to multiple parameters, especially for slotted anodes. It is one of the reasons why these different works are reported for idealised configurations since the anodes were perfectly horizontal with square edges as well as a square sidewall geometry, which is not necessarily directly relevant to industrial cells.

In the present paper, a numerical model based on turbulent flow coupled with phase transport physics is proposed with the intention of increasing the understanding of the role of slotted anodes on the evacuation of the gas phase generated at its bottom surface, the mixing in the central channel, and heat transfer in the side channel. This is obtained by evaluating the bath

hydrodynamics as well as the gas phase redistribution through different channels after its generation underneath the anode, considering the anode rounding induced by the concentration of the electric current at anode edges. The anode rounding used was measured on a cut-out cell. Different configurations of slotted anodes are investigated in the study. Starting with a description of the mathematical model, the various configurations are described afterwards. Subsequently, the first results obtained by the model and its validation with experimental data from the literature are presented. The last section is devoted to discussion and analysis of different cases simulated.

2. Numerical Setup

2.1 Governing Equations

As cited above, bubble generation below the anode induces turbulence of the bath in an aluminum reduction cell. For that, our numerical work is based on a 3D transient, weakly incompressible turbulent multiphase flow. The CFD model consists of coupling turbulent flow and phase transport physics. The latter solves the phase transport equation and obtains the gas volume fraction distribution in the computational domain, while the former gives principally the velocity and pressure profiles by solving the Navier-Stokes equations. The equations are:

- **Mass conservation**

$$\frac{\partial \rho}{\partial t} + \nabla.(\rho u) = 0 \tag{1}$$

- **Momentum conservation**

$$\rho \frac{\partial u}{\partial t} + \rho(u.\nabla)u = \nabla.[-pI + K] + \rho g + \sum F_{ext} \tag{2}$$

where:

ρ	Density,
u	Velocity
p	Pressure
t	Time
g	Acceleration of gravity
I	Identity matrix
$\sum F_{ext}$	Other external forces applied in the computational domain.

The term K is defined as:

$$K = (\mu + \mu_T)(\nabla u + (\nabla u)^T) - \frac{2}{3}(\mu + \mu_T)(\nabla.u)I - \frac{2}{3}\rho k I \tag{3}$$

Here:

μ, μ_T	Molecular and turbulent viscosity, respectively
k	Turbulent kinetic energy

In our study, in addition to the gravity force (ρg), a drag force between bubbles and the bath is considered, and solved by Haider and Levenspiel correlation [13]. In this study, we used a bubble diameter of 15 mm. This choice was based on the fact that a range of bubble diameters from 5 mm to 20 mm is commonly used in the literature [6], [7] and [16]. We carried out a series of numerical simulations using our CFD model where it is found that the results were only slightly different for the different tested bubble diameters (5 mm, 10 mm, 15 mm, and 20 mm).

- **Turbulence model**

The standard k-ε turbulence model is used as described in equations (4-7).

$$\rho\frac{\partial k}{\partial t}+\rho(u.\nabla)k=\nabla.\left[\left(\mu+\frac{\mu_T}{\sigma_k}\right)\nabla k\right]+P_k-\rho\varepsilon \quad (4)$$

$$\rho\frac{\partial \varepsilon}{\partial t}+\rho(u.\nabla)\varepsilon=\nabla.\left[\left(\mu+\frac{\mu_T}{\sigma_\varepsilon}\right)\nabla \varepsilon\right]+C_{\varepsilon 1}\frac{\varepsilon}{k}P_k-C_{\varepsilon 2}\rho\frac{\varepsilon^2}{k} \quad (5)$$

where:

$$\mu_T=\rho C_\mu\frac{k^2}{\varepsilon} \quad (6)$$

$$P_k=\mu_T\left[\nabla u:\left(\nabla u+(\nabla u)^T-\frac{2}{3}(\nabla.u)^2\right)\right]-\frac{2}{3}\rho k\nabla.u \quad (7)$$

where:

ε Turbulent kinetic energy dissipation rate,

The default values of the different turbulence model constants used in the equations (4) and (5) are: $C_{\varepsilon 1}=1.44$, $C_{\varepsilon 2}=1.92$, $C_\mu=0.09$, $\sigma_k=1.0$, $\sigma_\varepsilon=1.3$.

- **Phase transport equation**

To study the dynamics of a dispersed phase (bubbles, droplets, or solid particles) in another viscous fluid (where both fluids are immiscible), phase transport physics could be used through COMSOL Multiphysics. This interface deals principally with the resolution of the average volume fraction of phases and does not track the interface between different phases. Both interfaces are based on the macroscopic mass conservation equations of each phase [14]. The transport equation characterising the phase transport interface is:

$$\frac{\partial \rho_{s_i}s_i}{\partial t}+\nabla.N_i=0 \quad (8)$$

where:

ρ_{s_i} and s_i Density and volume fraction of each phase in the computational domain, respectively.

2.2 Boundary Conditions

The boundary conditions used for the solution of the differential equations cited above are:

- Inlet mass flux of generated CO_2 at the bottom surface of the anode with a released quantity of 0.00117 kg/m^{2}s per anode (without slots), corresponding to the gas quantity released from anode at a current density of 1.0 A/cm^2 for a chosen cell technology;
- At the top surface of the bath, a gas flux outlet has been imposed which allows the gas to escape with inlet rate;
- Slip condition on the gas inlet and outlet pre-cited;
- The remaining walls are supposed to be satisfying the non-slip condition.
- For slotted configurations, a slip condition is applied to the slot walls. The slot walls are assumed to be covered or partially covered with gas evacuated from the bottom surface of the anode.

The 3D Cartesian system is used to solve the governing equations (turbulent Navier-Stokes and phase transport equations) subject to the boundary conditions mentioned above. The commercial CFD software COMSOL Multiphysics is used. The continuous phase containing gas bubbles are discretised into several triangular finite elements. To optimise the computational time and memory power, a symmetry is assumed in simulations presented in the second section of the results discussion. The solver uses a finite element-based code to calculate the values of the velocity, pressure, and volume fraction at each node. An Algebraic Multigrid Method (AMG) solver is used together with a time-dependent second order backward differentiation formula (BDF) to determine each time step. The computational domain is discretised into a mesh,

composed of 2 million elements (when using symmetry) or 3.5 million elements (for full anode configurations).

3. Results and Discussion

3.1 Model Validation

To validate the CFD model, the numerical results were compared to experiments of Cooksey and Yang [7]. As cited before, these researchers [7] studied the impact of air bubble-induced turbulence on the hydrodynamics of the continuous phase (water). The generation of the dispersed phase was simulated by injecting air from the bottom surface of the three anodes set up in the experimental bench (120 L/min for each anode). PIV technique was used to measure the flow dynamics at the centre and side channel along three planes: at the mid-point of each inter-anode gap and at the mid-point of the slot situated at the centre of the middle anode. In their study, the researchers [7] worked with three anodes to be able to consider that the central anode is almost isolated.

Figure 1 presents snapshots comparing water mean velocity vector and streamlines obtained experimentally [7], and by our numerical model.

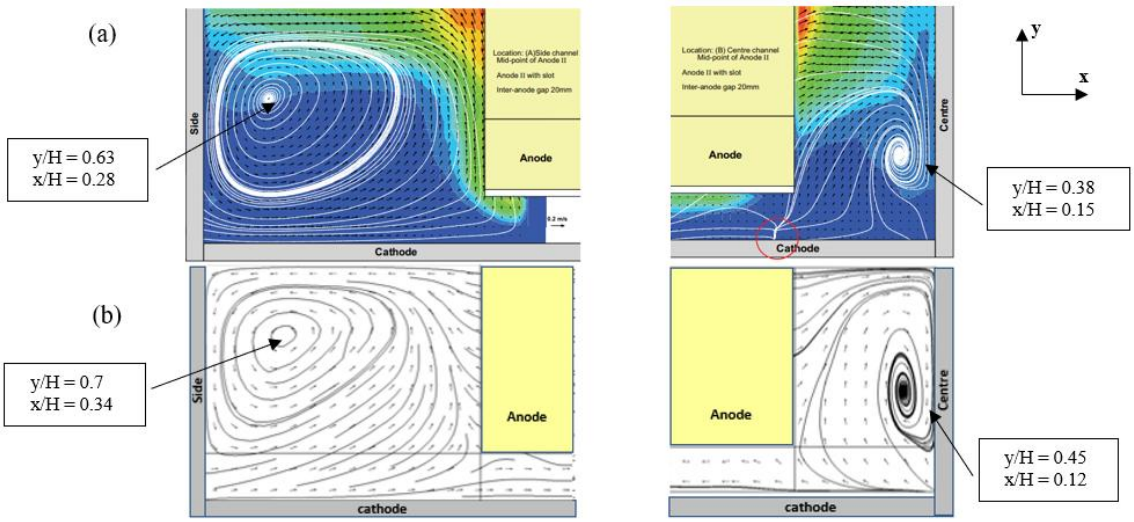

Figure 1. Velocity vectors and streamlines obtained from side channel and central channel at the mid-point of the slot. (a) experimentally [7]; (b) our numerical model. With H (bath height including ACD) = 0.2 m, x and y are the coordinates of the recirculation zone.

As depicted in the Figure 1, results are obtained from two locations (side channel and central channel) at the mid-point of the slot. For the recirculation zone position, it is remarked that it was experimentally determined to be at $y^*\left(\frac{y}{H}\right) = 0.63$ and $x^*\left(\frac{x}{H}\right) = 0.28$ in the side channel and $y^* = 0.38$ and $x^* = 0.15$ in the central channel. Numerical simulations found that the recirculation zone was located at $y^* = 0.7$ and $x^* = 0.34$ in the side channel, and $y^* = 0.45$ and $x^* = 0.12$ in the centre channel. A good agreement is found comparing numerical results obtained by our model and experiments for anodes with open slots configuration, as cited in [7].

For the same experimental bench cited above and for anodes without slots, Figure 2 presents the velocity vectors together with streamlines at the mid-point of the ACD obtained, on one hand numerically with the elaborated model and, on the other hand experimentally by Feng et al., [6]. A good similarity for the flow patterns between numerical and experimental results is remarked.

Overall, the elaborated model and experiments are in a good agreement for different configurations (without slots and with open slots). This gives the model the ability to be used in next sections.

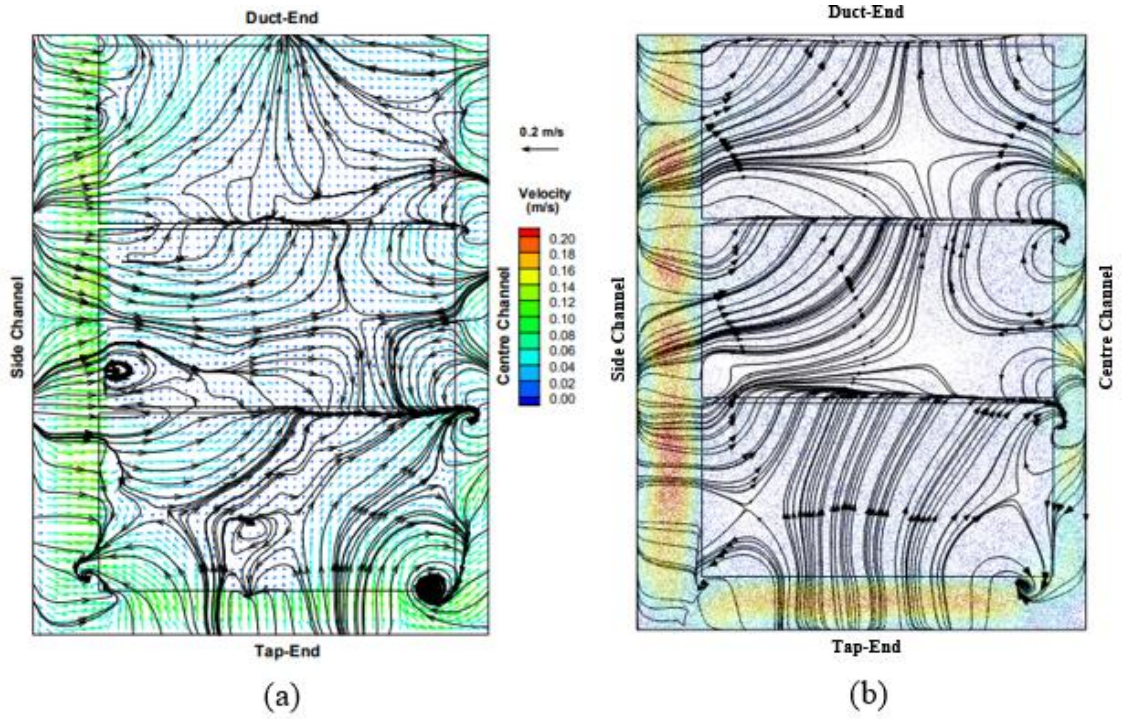

Figure 2. Water velocity distribution at the mid-point of the ACD: a) experimental work; b) our numerical result.

In the next sections, the model will be used for further numerical simulations investigating the impact of anode configuration together with the thickness and inclination of used slots on the hydrodynamics of the bath, as well as on the redistribution of the gas phase released from its bottom surface. Anode length was 1690 mm and width 685 mm. Bath height was 180 mm (including the ACD of 30 mm). Rounding of different edges are fixed to be 50 mm radius, which was measured on some cell autopsies.

3.2 Impact of Anode Configuration

For the same number of slots (2 slots per anode) and slot thickness (11 mm), Figure 3 shows three-anode configurations with different slot directions (longitudinal, transversal and diagonal), that were investigated to check the effect of bubbles on bath flow as well as the redistribution of the gas through different channels around the anodes (centre channel, side channel, and inter-anode gap). In this section, slots are not inclined.

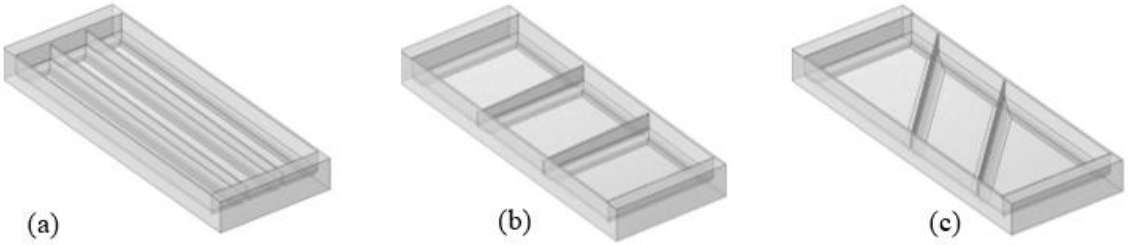

Figure 3. Different slotted anode configurations; a) longitudinal slots; b) transversal slots; c) fully diagonal slots.

Figure 4 presents the gas volume fraction distribution in the computational domain for each configuration cited in Figure 3. It is observed that the concentration of the gas underneath the anode is greater for anodes with transversal and diagonal slots than for the anode with longitudinal slots which is in line with results of previous research [16].

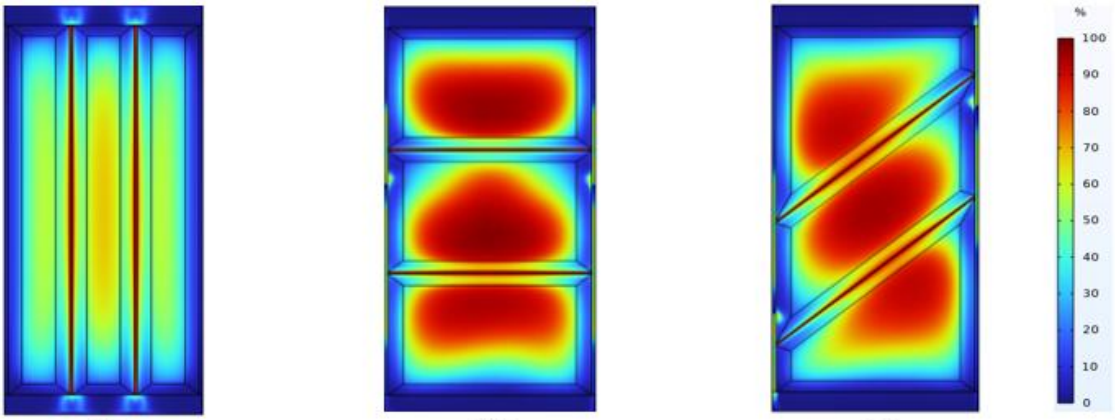

Figure 4. Gas volume fraction distribution at the bottom surface of different slotted anode configurations; a) longitudinal slots; b) transversal slots; c) fully diagonal slots.

This is due to the fact that the space available for gas flow in transversal or diagonal slots is smaller than in longitudinal slots. This provokes quick saturation of the slot volume by the released gas, keeping the bubbles under the anode for a longer time and forcing them to coalesce, grow and form a thin gas layer. On the other hand, the gas escapes easily through the shorter path underneath the anode to the slots in longitudinally-slotted anodes.

It is worth to mention that in previous studies it was shown that when big bubbles coalesce, they take on a round shape. The narrow unslotted area limits the formation of larger bubbles, causing them to escape more easily and quickly. In our model, bubbles coalescence and rupture are not considered because our model is limited to model the average volume fraction of phases and does not track the interface between different phases.

In addition to removing gases generated underneath the anodes, increased mixing and dissolution of alumina is also expected in the central channel. Figure 5 shows the amount of gas passing through central and side channels for different anode configurations. The configurations include anode without slots, anode with open transversal slots, and anodes with immersed transversal, longitudinal and diagonal slots. It is noteworthy that all slots used in this section are not inclined. It is shown that immersed longitudinal slots pass a higher amount of gas through central and side channels than other configurations. This enhances remarkably the bath mixing rate in the central and side channels with longitudinal slots. It is remarked that open longitudinal slots anode allows the least amount of gas passing through surrounding channels. This is mainly because most of the generated gas is drawn through the open slots and inter-anode gaps to the free surface, which limit considerably the gas quantity passing through central and side channels. However, when these longitudinal slots are immersed, their top surface become an obstacle for the gas released from the bottom surface of the anode. This causes the gas to be directed through the surrounding channels, which explains the higher amount of gas that passes through the central and side channels.

On the opposite side, to control the heat balance at the ledge side, the mixing rate at the side channel should not be as intense as at the central channel where an optimisation of the slot shape must be considered in the design of the anode to minimise such effect. In the next section, the

impact of different slots design parameters is investigated and discussed for not inclined anodes (downstream).

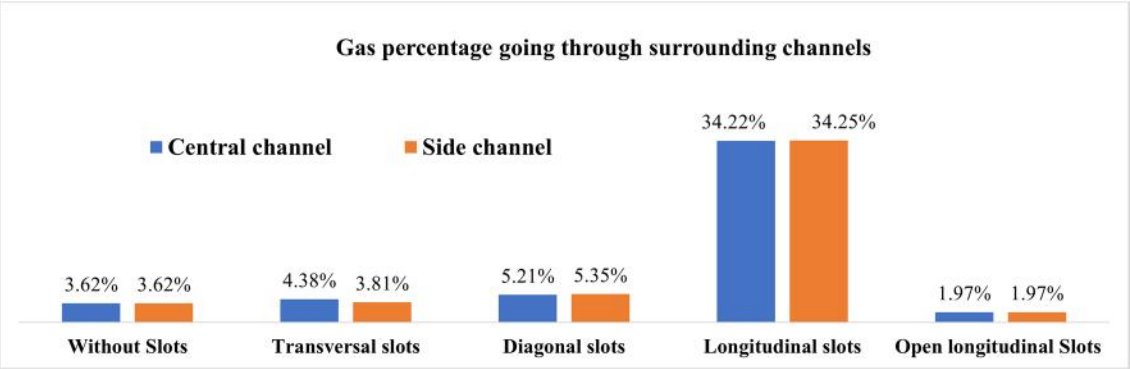

Figure 5. Gas redistribution through the surrounding channels corresponding to each configuration used in the study.

3.3 Impact of the Slot Thickness and Inclination

In this section, we continue our investigation with an anode that has longitudinal slots which is an industrial standard now. This configuration has shown better results as seen above in terms of bubble evacuation and gas redistribution to surrounding channels. Therefore, we will explore further its potential in function of slot thickness and inclination. As can be seen from figures below, symmetry about the longitudinal axis of the anode was applied in these configurations. Different inclinations (20 mm, 40 mm, and 80 mm) and thicknesses (8 mm, 11 mm, and 22 mm) were tested.

3.3.1 Influence of Slot Inclination for 11 mm Slot Thickness

Figure 6 shows the distribution of the gas volume faction in the computational domain for a fixed slot thickness of 11 mm and different slots inclinations.

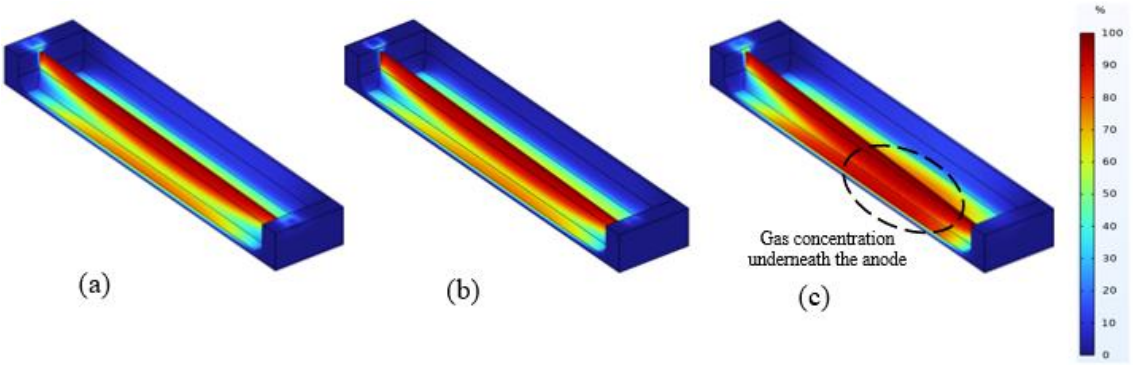

Figure 6. Anode with different longitudinal slot inclinations; a) 20 mm; b) 40mm; c) 80 mm.

It is observed that the gas phase tends to concentrate in a certain region underneath the anode as the inclination of the slots increases (as in Figure 6c). This is caused by the fact that the evacuation space generated by the slot becomes smaller for higher inclinations, which results in the saturation of the slot with gas. This forces the generated gas to remain in the bottom surface of the anode for longer time, especially in the region where the inclination is the highest. This leads to an increase in the coverage of the gas in this region as presented in Figure 7 and can lead to increase of bubble layer voltage drop for older anodes when slots are immersed into the bath.

The impact of the slot inclination is also observed in the redistribution of the gas to different surrounding channels (mainly the central and side channels). Figure 8 shows the variation of the amount of gas evacuated through the central and side channels as a function of the slot inclination for a constant thickness of 11 mm. It is observed that without slot inclination, the amount of gas that passes through the central and side channels is approximately the same (35 %). This distribution starts to change with the inclination of the slots, to ~ 42 % (in central channel) when the slot is inclined by 80 mm. In parallel, the amount of gas that passes through the side channel decreases from approximately 35 % (with no slot inclination) to ~ 20 % in the 80 mm inclined slot. This provokes, as well, a remarkable changing in the velocity profile adjacent to the ledge at the side wall as shown in Figure 9. These results are important for heat balance on the side walls where lower bath mixing will promote a thicker ledge. One way to prove this would be to use a coupled CFD-heat transfer model which would predict the heat balance around the ledge.

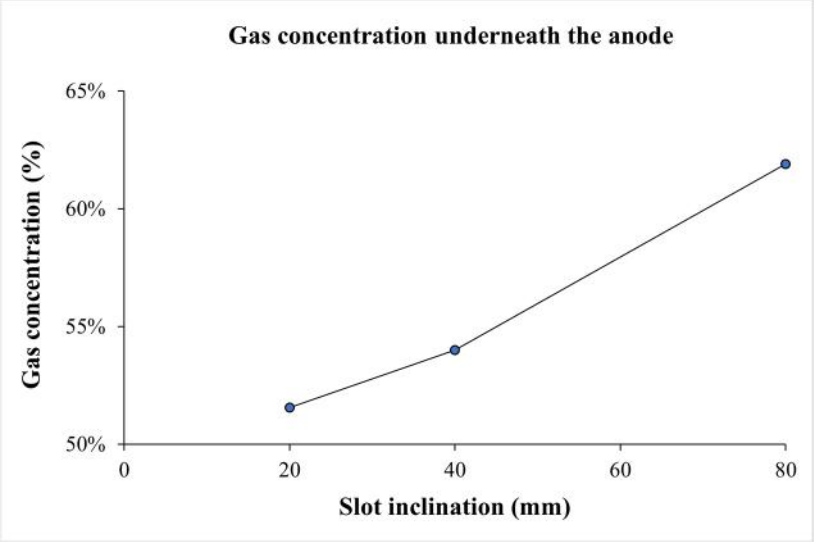

Figure 7. Variation of the gas concentration underneath the anode for different slot inclinations; 20 mm; 40 mm; and 80 mm.

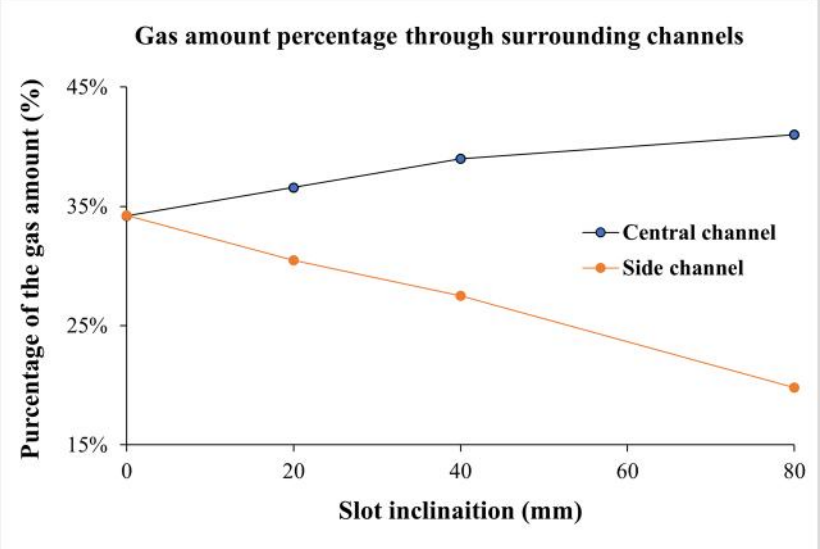

Figure 8. Impact of the slot inclination (20 mm, 40 mm, and 80 mm) on the redistribution of the released gas from the bottom surface of the anode through the central and side channel.

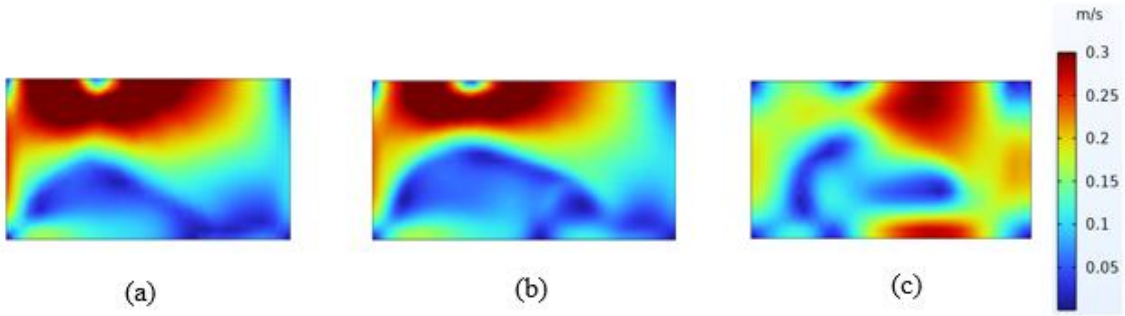

Figure 9. Velocity profile at the side wall (ledge) for different slot inclinations; a) 20 mm; b) 40 mm; c) 80 mm.

3.3.2 Influence of Slot Thickness for Slot Inclination of 20 mm

Fixing the slot inclination at 20 mm, Figure 10 presents anodes with different slot thicknesses that were investigated in this section.

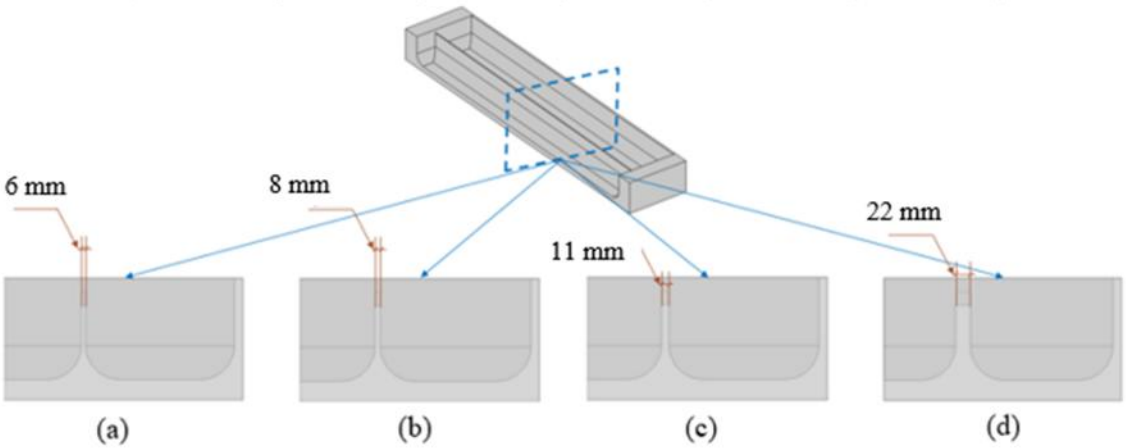

Figure 10. Anode with different longitudinal slot thicknesses: a) 6 mm; b) 8 mm; c) 11 mm; d) 22 mm.

It is found that the enlargement of the slot space helps decreasing the gas volume fraction concentrated underneath the anode. As explained previously, this is due principally to the fact that for thicker slots the volume containing the gas is large which helps to suck more gas from the bottom surface of the anode to the slots. For open and immersed anode slots, Figure 11 illustrates the distribution of the gas concentration underneath the anode in function of the slot thickness. It is shown that for both cases (open and immersed slots), the gas concentration at the bottom surface of the anode decreases with the increasing slot thickness. In parallel, comparing results obtained for immersed slots with those obtained for open slots, it is shown that using open slots the bubble concentration under the anode is smaller than for immersed slots (~67 % vs. ~49 % for the narrowest slots of 6 mm, and ~43 % vs. ~38 % for 22 mm wide slots), as presented in Figure 12. This is due principally to the fact that open slots are not saturated with gas (free surface) which allows continuous evacuation of bubbles through the slot space, similar to the one happening at the inter-anode gap.

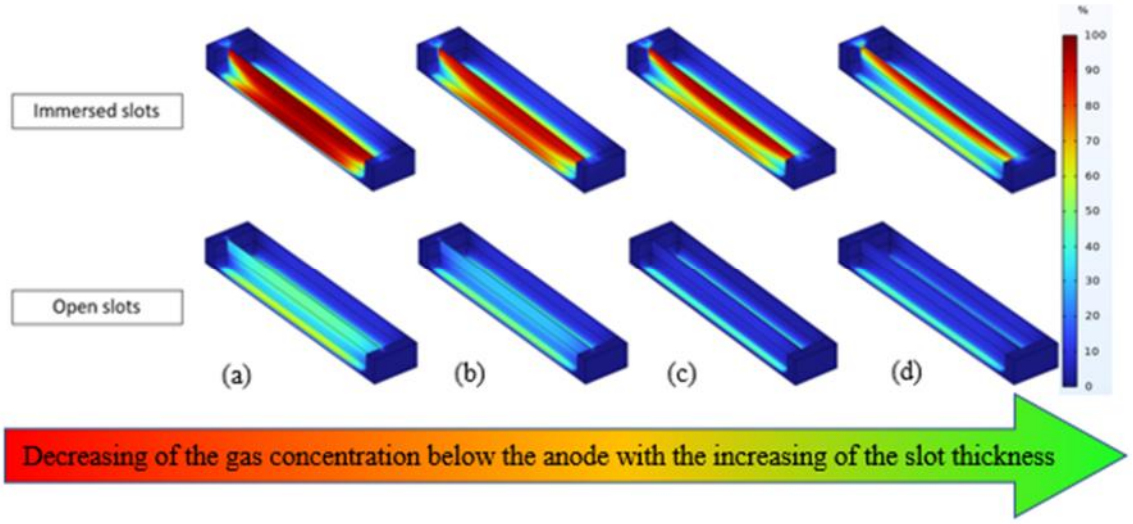

Figure 11. Distribution of the gas volume fraction in the computational domain for anode with different slot thicknesses: a) 6 mm; b) 8 mm; c) 11 mm; d) 22 mm.

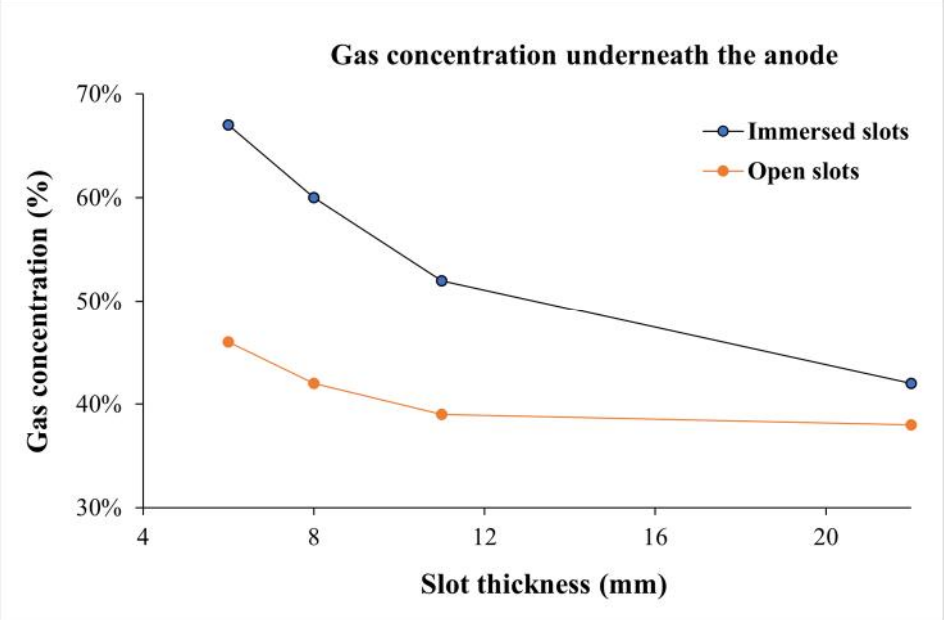

Figure 12. Variation of the gas concentration underneath the anode function of the slot thickness.

Figures 13 and 14 show velocity profile and streamlines at the mid-point of an immersed slot and an open slot, respectively, at distinct locations (central and side channel) for the different thicknesses evaluated in this section. It is shown, for both cases, that the slot thickness may have an impact on the bath recirculation intensity since the exit velocity from the slot is higher in case of narrow slots than in case of larger slots (perpendicular surface to the flow direction is smaller for narrow slots than for larger slots). Focusing on the side wall view (ledge), it is remarked that the slot thickness impacts slightly the velocity profile for both cases. This is explained by the fact that the exhausting velocity of the bath from the slot is higher for narrower slots than thicker slots as explained above which gives the bath more kinetic energy when using narrow slots than thick slots. It is also important to mention that the impact of open slots on the side channel (ledge) is less than that of immersed slots. This is because the gas released from the bottom surface of the anode is redirected through the surrounding channels when the slot is immersed. This redirection

of gas results in a higher gas quantity passing through the central and side channels in the immersed slot case than in the open slot case as seen before. The results discussed about the impact of slots on bath hydrodynamics in the side channel suggest that the slot height (immersed or open) has some impact on the heat balance of the cell (side ledge).

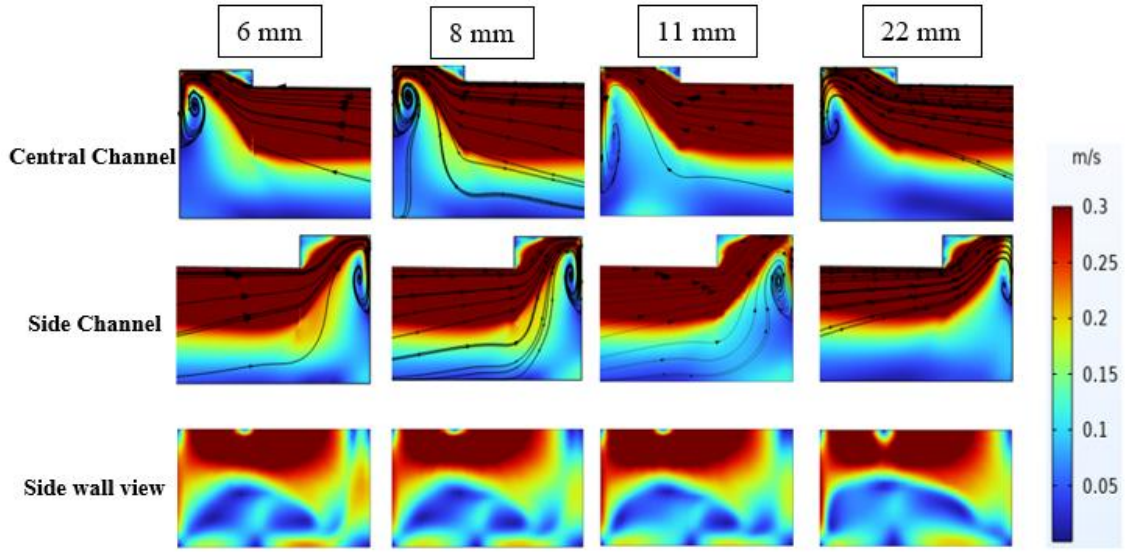

Figure 13. Velocity profiles and streamlines at the mid-point of an immersed slot in central and side channels as well as at the side wall (ledge) function of the slot thickness.

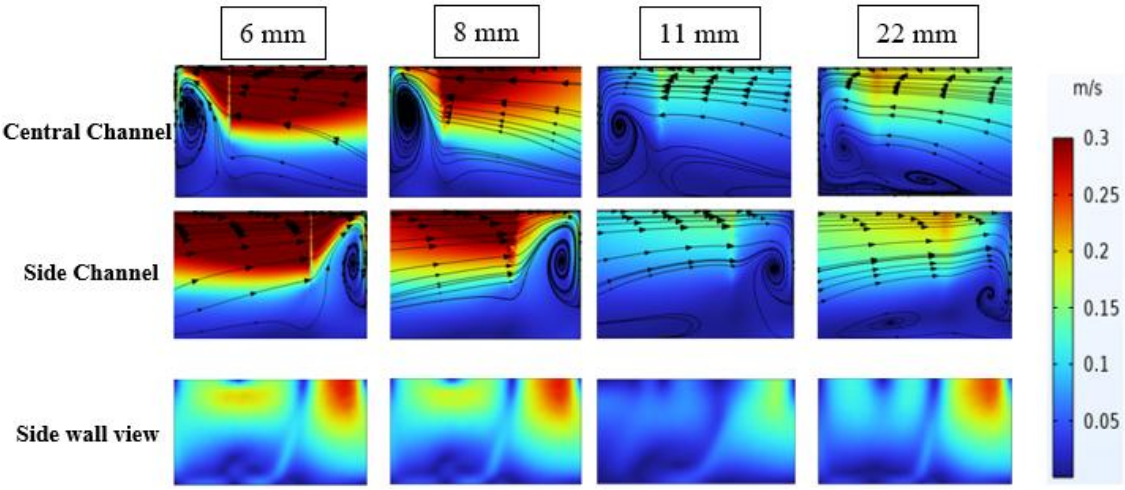

Figure 14. Velocity profiles and streamlines at the mid-point of an open slot at the central and side channels as well as at the side wall (ledge) function of the slot thickness.

Figure 15 shows the variation in the amount of gas evacuated through the central and side channels for different slot thicknesses for immersed and open slots. For immersed slots (Figure 15a), results show that increasing the slot thickness from 6 mm to 22 mm significantly increases (by approximately 12 %) in the amount of gas evacuated through the central channel, but a smaller increase (by approximately 4 %) in the amount of gas exhausted through the side channel is observed. This means that for thicker slots, a substantial additional amount of gas is directed through the central channel and not to the side channel. When using open slots (Figure 15b), the generated gas is evacuated perpendicularly (through the open slot and inter-anode gap) to the free surface, as seen before. This lowers the gas quantity escaping through the central and side channels compared to the first case when the slots are immersed. It is found from Figure 15b that the quantity of the gas passing through central and side channels is equal and varies from ~7 %

for narrowest slots (6 mm) to ~2.0 % for 11 mm slot thickness. This decrease is due to the difference in kinetic energy for the evacuated bath from the slot where the narrowest slots induce higher kinetic energy as explained before.

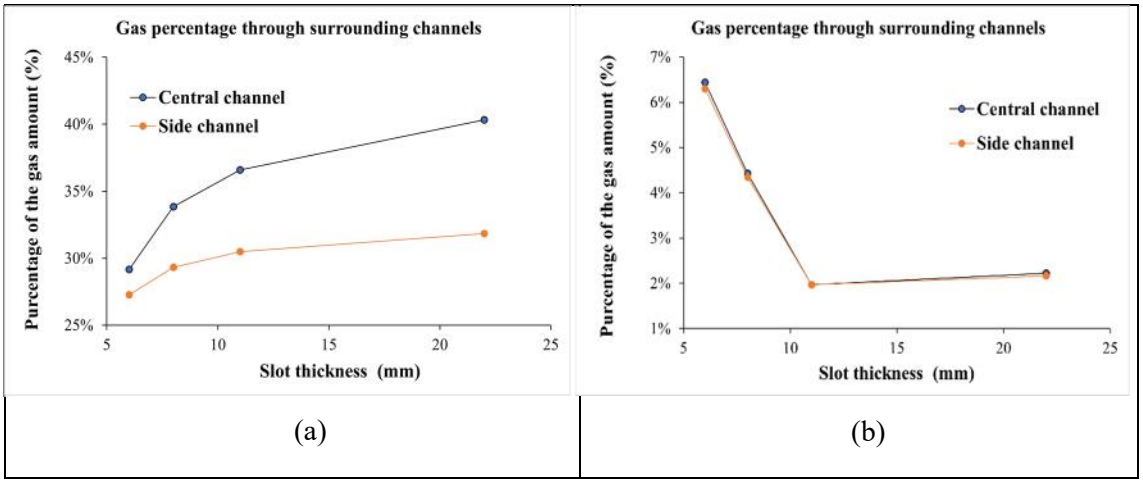

(a) (b)

Figure 15. Gas percentage through surrounding channels function of the slot thickness for: a) immersed slots; b) open slots.

It is worth mentioning that the gas quantity passing through surrounding channels gets slightly higher from ~2.0 % for 11 mm slot thickness to ~2.3 % for 22 mm thickness. This could explain the behaviour of the velocity at the ledge side when slots are open (Figure 14) where it was found that using slots of 11 mm thickness has less impact on the side channel (ledge) that when a thicker slot of 22 mm is used.

4. Conclusions

In this paper, we presented a numerical study of the impact of anode slot design on the gas evacuation and redistribution of electrolysis gases (mainly CO_2) generated at the bottom surface of the carbon anode block inside an aluminium electrolysis cell. We investigated different slot inclinations (20 mm, 40 mm, and 80 mm) and thicknesses (6 mm, 8 mm, 11 mm, and 22 mm) using a computational fluid dynamics (CFD) model, built in COMSOL Multiphysics, coupled with a turbulent flow and phase transport physics. Our results show that the longitudinal slots are more effective for evacuating the gas and redistributing it through different channels than transversal or diagonal slots. This is because longitudinal slots create a shorter path for the gas to be removed from the bottom surface of the anode and provide a larger volume for gas to escape through. This also helps to create a more uniform flow of bath around the anode.

Regarding slot inclination, it is found that the more the slot is inclined the more the gas is directed through the central channel instead of the side channel. Higher slot inclination decreases bath stirring in the side channel and increases the side ledge stability; a detailed CFD and heat transfer model would be required to simulate this aspect.

It is shown as well that the thickness of the slot affects the distribution of the gas. Thicker slots allow better gas removal from the bottom of the anode, which can lead to a decrease in the gas concentration underneath, lowering bubble voltage drop.

Open slots lead to the gas generated underneath the anode to be removed continuously from the bottom surface of the anode which prevents its saturation. But this can be a penalty for bath mixing and alumina dissolution as the quantity of the gas evacuated through the central channel (helpful for alumina mixing) is dramatically reduced compared to the case where slots are immersed.

The results of this study can be used to optimise the design of anode slots in aluminium reduction cells. By understanding the impact of slot inclination and thickness on gas distribution together with the bath mixing in the central channel and heat transfer at the side channel, it is possible to design slots that improve the efficiency of the cell by better alumina dissolution, lowering bubble voltage drop and to reduce the risk of premature cell failure with a better ledge covering of the side walls.

5. References

1. Torstein Haarberg, Asbjørn Solheim and Stein Tore Johansen, Effect of anodic gas release on current efficiency in Hall-Heroult cells, *Light Metals* 1998. 475-482.
2. László I. Kiss, Transport processes and bubble driven flow in the Hall-Héroult cell, *Fifth International Conference on CFD in the Process Industries CSIRO,* 13-15 December 2006, Melbourne, Australia.
3. Kristian Etienne Einarsrud, Stein Tore Johansen and Ingo Eick, Anodic bubble behaviour in Hall-Héroult cells, *Light Metals,* 2012, 875-880.
4. Alton T. Tabereaux and Ray D. Peterson, *Treatise on Process Metallurgy: Industrial Processes*. *Industrial Processes,* Chapter 2.5 - Aluminum Production*,* Volume 3: Industrial processes, 2014, 839-917.
5. Zhibin Zhao et al., Numerical modeling of flow dynamics in the aluminum smelting process: comparison between air–water and CO_2–cryolite systems, *Metall Mater Trans B* 48 2017, 1200–1216, *https://doi.org/10.1007/s11663-016-0872-x* .
6. Yuqing Feng, William Yang, Mark Cooksey and Phil Schwarz, CFD model of bubble driven flow in aluminium reduction cells and validation using PIV measurement, *International Journal of Heat and Mass Transfer*, 2010, vol. 53, no. 21–22, Pages 4769–4778.
7. Mark Cooksey and William Yang, PIV measurements on physical models of aluminium reduction cells, *Light Metals* 2006, 359-365.
8. Yipeng Huang et al., Bingliang Gao et al., Anodic bubble behavior in a laboratory scale transparent electrolytic cell for aluminum electrolysis, *Metals,* 2018, 8 (10), 806, https://doi.org/10.3390/met8100806.
9. Liang Wang et al., Numerical modeling of effect of slot on bubble motion in aluminum electrolytic process, *Trans. Nonferrous Met. Soc. China* 28, 2018, 1670−1678.
10. Meijia Sun, Bao-kuan Li, Zhongqiu Liu, Lixin Tang, Experimental and numerical investigations on transient multiscale bubble behaviors in $CuSO_4$ aqueous solution electrolysis cell, *Chemical Engineering Journal,* 2022, Volume 428, 131182.
11. Rainier Hreiz et al., Bubbles induced convection in narrow vertical cells: A review, *J. Chemical Engineering Research and Design*, 2015, 100 (10): Pages 268−281.
12. Rainier Hreiz et al., Electrogenerated bubbles induced convection in narrow vertical cells: PIV measurements and Euler–Lagrange CFD simulation, *Chemical Engineering Science*, 2015, 138-152.
13. Liang Wang et al., Effect of gas bubble on cell voltage oscillations based on equivalent circuit simulation in aluminum electrolysis cell, *J. Transactions of Nonferrous Metals Society of China*, 2015, 25 (1), Pages 335−344.
14. Meijia Sun et al., Effect of slotted anode on gas bubble behaviors in aluminum reduction cell, Metall Mater Trans B 48 2017, 3161–3173. https://doi.org/10.1007/s11663-017-1065-y .
15. Meijia Sun, Baokuan Li, Linmin Li, A multi-scale mathematical model of growth and coalescence of bubbles beneath the anode in an aluminum reduction cell, *Metall Mater Trans B* 49 2018, 2821–2834, https://doi.org/10.1007/s11663-018-1311-y.
16. Dagoberto S. Severo, Vanderlei Gusberti et al., Modeling the bubble driven flow in the electrolyte as a tool for slotted anode design improvement, *Light Metals* 2007, 287-292.